



Universal mechanical instabilities in the energy landscape of amorphous solids: Evidence from athermal quasistatic expansion

Umang A. Dattani ^{1,2}, Smarajit Karmakar ³, and Pinaki Chaudhuri ^{1,2}

¹The Institute of Mathematical Sciences, CIT Campus, Taramani, Chennai 600113, India

²Homi Bhabha National Institute, Anushaktinagar, Mumbai 400094, India

³Tata Institute of Fundamental Research, 36/P,

Gopanpally Village, Serilingampally Mandal, Ranga Reddy District, Hyderabad, 500107 Telangana, India



(Received 24 December 2021; revised 28 October 2022; accepted 2 November 2022; published 28 November 2022)

Using numerical simulations, we study the failure of an amorphous solid under athermal quasistatic expansion starting from a homogeneous high-density state. During the expansion process, plastic instabilities occur, manifested via sudden jumps in pressure and energy, with the largest event happening via cavitation leading to the material's yielding. We demonstrate that all these plastic events are characterized by saddle-node bifurcation, during which the smallest nonzero eigenvalue of the Hessian matrix vanishes via a square-root singularity. We find that after yielding and prior to complete fracture, the statistics of pressure or energy jumps corresponding to the plastic events show subextensive system-size scaling, similar to the case of simple shear but with different exponents. Thus, overall, our paper reveals universal features in the fundamental characteristics during mechanical failure in amorphous solids under any quasistatic deformation protocol.

DOI: [10.1103/PhysRevE.106.055004](https://doi.org/10.1103/PhysRevE.106.055004)

I. INTRODUCTION

Amorphous solids are extensively utilized in diverse applications that span from nanometric scales to centimeters [1–4]. Stability of these materials under various external mechanical perturbations is important for such usage, and hence the significance for understanding the underlying processes leading to their mechanical failure. Cavitation is one such mode of spontaneous catastrophic failure that occurs in these solids, be it hard (metallic glass, polymer glass etc.) or soft (emulsions, wet granular matter, gels, etc.), when the material is subjected to expansion of some kind. The initial microcavities [5–16] potentially lead to eventual fracture if the expansion process is continued, as evidenced in recent experiments [17]. Thermodynamically, formation of cavities is related to accessing the zone of solid-gas coexistence in the temperature-density plane of the phase diagram of cohesive glass-forming systems [18–20], as encountered both at finite temperatures [21–23] and under athermal conditions [18] during mechanical expansion.

The underlying energy landscape of amorphous materials is complex, and analyzing the material properties through the landscape's features, especially the local minima [called inherent structures (ISs)] and saddles, is a domain of active research. In the context of the material's response to athermal quasistatic shear (AQS) [2,24], i.e., at vanishing driving rate and in the absence of thermal noise [25,26], it has been demonstrated that, during the straining process, yielding happens via the occurrence of irreversible plastic events and each such event can be considered as a catastrophic process corresponding to a saddle node bifurcation within the energy landscape, i.e., whenever an event occurs, the smallest nonzero eigenvalue of the Hessian matrix, $\mathcal{H}_{ij}^{\alpha\beta}$ (defined later)

vanishes via a square-root singularity [24,27–30]. Appearance of the square-root singularity is special, particularly because a minimum and a saddle of index 1 in the underlying potential energy landscape have to meet each other during the deformation process, leading to a saddle-node bifurcation. Here saddle of index 1 refers to the saddle in the energy landscape which has one unstable direction. The failure via saddle of index 1 is one of the crucial aspects of this deformation process, as it means the vanishing of only the lowest nonzero eigenvalue in this context. For example, if the process happens via a saddle of index 2, then it would have meant that two eigenvalues would have simultaneously gone to zero at the failure point. Thus, saddle-node bifurcation is very special, as it means that deformation proceeds along a unique direction, the direction of the lowest eigenvector. This also means that particles in the whole system move in a concerted manner along the direction of the lowest eigenvector. To reiterate, this process is not necessarily the same in other deformation processes across different systems, for example, in a granular assembly of spheres in the presence of frictional forces, the plastic event leads to a different bifurcation process, and it has been demonstrated in Ref. [31] that two real eigenvalues can merge and give rise to two imaginary eigenvalue pairs instead of vanishing of the lowest eigenvalue.

Further, analyzing the statistical properties of the plastic events is also of significance. In the case of the AQS steady state, it has been shown [30] that the mean drops in energy and stress, respectively, scale as $\langle\Delta U\rangle\sim N^\alpha$, $\langle\Delta\sigma\rangle\sim N^\beta$, where $\alpha=1/3$ and $\beta=-2/3$, being universal exponents in both two and three dimensions across different model systems.

It is pertinent to ask whether other quasistatic mechanical deformations also involve similar singularities and follow similar statistics. *A priori*, it is not evident that spontaneous

emergence of density inhomogeneities in the form of cavity formation, under expansion, would correspond to a failure via saddle of index 1. A recent study using a one-component system, which potentially crystallizes at low temperatures, seemed to show that at the instant of cavitation of the solid, a saddle-node bifurcation does occur [32]. However, the study specifically focused near the Sastry density, i.e., where IS states start to show spatial inhomogeneities [33,34], using states obtained through thermal quench from a high-temperature liquid state at this density and then probing its stability. The behavior at higher or lower densities and specifically IS states sampled at low temperatures was not studied.

In this paper, we investigate the stability of local minima within the energy landscape visited by a model amorphous solid while it is subjected to athermal quasistatic expansion (AQE), starting from a homogeneous high-density state. We observe that the expansion leads to the release of pressure via spontaneous formation of cavities, which become precursors for fracture progression upon continued expansion, and eventually leads to loss of material integrity. We demonstrate that, all throughout this trajectory, plastic events of different magnitudes happen, be it in the homogeneous state or when density inhomogeneities pop up and proliferate. And, all such events occur via a saddle node bifurcation within the energy landscape. Further, we show that during cavitation and prior to complete fracture, the statistics of pressure or energy jumps corresponding to the plastic events show subextensive system-size scaling [28], similar to the case of AQS but with different exponents. Thus, broadly speaking, our observations regarding the response to expansion in conjunction with previous observations on response to shear deformations indicate that the nature of mechanical instabilities that the underlying landscape of amorphous materials undergo under any mechanical deformation is universal in nature.

The paper is organized as follows. After the introductory discussions in Sec. I, we elaborate on the modeling aspects and numerical methods used in our study in Sec. II. This is followed by an extensive discussion of our findings in Sec. III, and we conclude with a summary and perspectives in Sec. IV.

II. MODEL AND METHODS

A. Model details and initial states

Our study is mainly focused on the well-characterized two-dimensional model binary Lennard-Jones mixture (KABLJ) which has 65 : 35 composition of the two species, labeled A and B , with interaction parameters and $\sigma_{AA} = 1.0$, $\sigma_{BB} = 0.88$, $\sigma_{AB} = 0.8$, $\epsilon_{AA} = 1.0$, $\epsilon_{BB} = 0.5$, $\epsilon_{AB} = 1.5$ [35]. In this model, the interaction potential, smoothed over to first two derivatives, between particles i and j is the following:

$$V(r_{ij}) = 4\epsilon_{ij} \left[\left(\frac{\sigma_{ij}}{r_{ij}} \right)^{12} - \left(\frac{\sigma_{ij}}{r_{ij}} \right)^6 \right] + u(r_{ij}), \quad (1)$$

where

$$u(r_{ij}) = C_0 + C_2 \left(\frac{r_{ij}}{\sigma_{ij}} \right)^2 + C_4 \left(\frac{r_{ij}}{\sigma_{ij}} \right)^4. \quad (2)$$

Here, i and j would correspond to either of the labels A or B . The constants C_0 , C_2 , and C_4 are determined by requiring

the potential and its first two derivatives to be zero at the cutoff $r = 2.5\sigma_{ij}$. The simulations have been performed for a variety of system sizes ranging from $N = 10^3$ to $N = 10^5$.

To prepare initial states for our study, we first equilibrate the system at $T = 1.0$ (in LJ units), which is in the liquid regime, followed by cooling at a constant rate of 10^{-4} per MD timestep to a final temperature of $T = 0.01$ [36], which is in the glassy regime. The corresponding glass transition temperature of the model system is at $T = 0.33$ [37]. The athermal states used in our paper are generated by obtaining IS states corresponding to the glassy configurations at $T = 0.01$, via conjugate gradient minimization.

We also study a few other models in $d = 2, 3$, detailed in the Supplemental Material (SM) [38], to demonstrate universal behavior across diverse model amorphous systems. These are: (i) The 3D Kob-Andersen (3dKABLJ) [35]: 80:20 binary mixture interacting via Lennard-Jones potential with the same interaction parameters as 2DMKA. The initial states were prepared by quenching high temperature ($T > 2.0$) liquid. (ii) 3D Wahnstorm mixture (3dWahn) [39]: 50:50 binary mixture interacting via Lennard-Jones potential with parameters, $\epsilon_{AA} = \epsilon_{BB} = \epsilon_{AB} = \sigma_{AA} = 1.0$, $\sigma_{AB} = 1.1$, and $\sigma_{BB} = 1.2$. The initial states were prepared by quenching high temperature ($T > 2.0$) liquid. (iii) 2D Lancon *et al.* model (2dLancon) [40,41]: A binary mixture with composition $N_A/N_B = (1 + \sqrt{5})/4$, interacting via Lennard-Jones potential with parameters $\sigma_{AA} = 2 \sin(\pi/5)$, $\sigma_{BB} = 2 \sin(\pi/10)$, $\sigma_{AB} = 1.0$, $\epsilon_{AA} = \epsilon_{BB} = 0.5$, and $\epsilon_{AB} = 1.0$. The initial states were prepared by quenching high temperature ($T > 3.0$) liquid.

B. Athermal quasistatic expansion and stability analysis

Starting from a spatially homogeneous high density state ($\rho = 1.2$ for KABLJ) having positive barostatic pressure, we study the athermal quasistatic response (i.e., in the absence of any thermal effects and in the limit of vanishing driving rates) of this system to isotropic expansion [18]. In each expansion step, a constant volume strain is applied on the system by rescaling the length of the box by a factor $(1 + \epsilon)$ along with affine transformation of particle coordinates, followed by minimization of the energy of this strained configuration using the conjugate gradient algorithm [42]. The values of ϵ are varied from $\epsilon = 10^{-4}$ to $\epsilon = 10^{-9}$. The initial states used for the expansion process are obtained by thermally cooling high-temperature liquid states, followed by energy minimization; see SM for further details. The AQE simulations are done using LAMMPS [43].

LAPACK [44] is used for doing the stability analysis of the local minima states by computing eigenvalues and eigenvectors of the Hessian matrix $\mathcal{H}_{ij}^{\alpha\beta}$, which is defined as

$$\mathcal{H}_{ij}^{\alpha\beta} = \frac{\partial^2 U(\{\mathbf{r}_i\})}{\partial r_i^\alpha \partial r_j^\beta}. \quad (3)$$

For a system of N particles interacting via a pairwise potential $\phi(r)$, the potential energy is given by

$$U(\mathbf{r}_1, \mathbf{r}_2, \dots, \mathbf{r}_N) = \frac{1}{2} \sum_{i=1}^N \sum_{j=1; i \neq j}^N \phi(|\mathbf{r}_i - \mathbf{r}_j|).$$

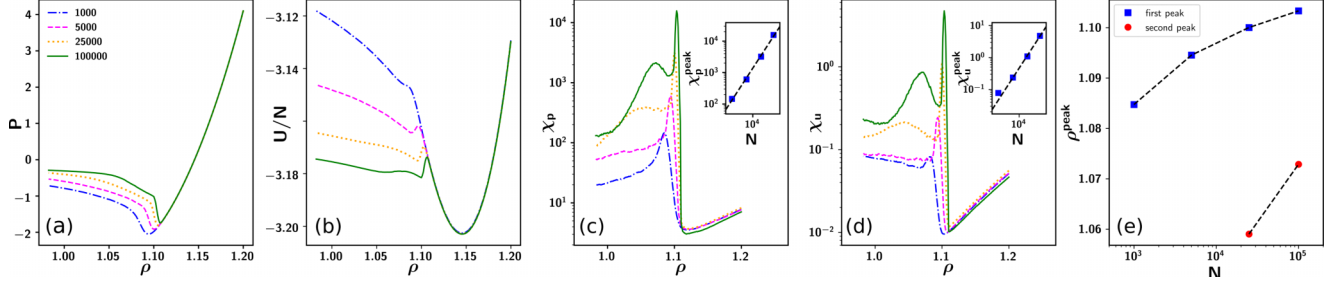


FIG. 1. Model KABLJ. Variation of (a) average pressure (P), (b) average energy per particle (U/N), with density ρ , for different system sizes as marked. Corresponding density variation of susceptibility (c) χ_p and (d) χ_u . Inset of (c) shows the system-size dependence of pressure susceptibility peak, $\chi_p^{\text{peak}} \sim N$, indicated with dashed line. Similar system size variation of χ_u^{peak} shown in inset of (d). (e) Density values at which the two peaks in susceptibility occur, for different system sizes.

The Hessian matrix of the potential energy for a pairwise potential can be reduced to [29]

$$\mathcal{H}_{\alpha\beta}^{ij} = \frac{\partial^2 U}{\partial \mathbf{r}_\alpha^i \partial \mathbf{r}_\beta^j} = - \left(\frac{\phi_{rr}^{ij}}{(r^{ij})^2} - \frac{\phi_r^{ij}}{(r^{ij})^3} \right) r_\alpha^i r_\beta^j - \delta_{\alpha\beta} \frac{\phi_r^{ij}}{r^{ij}}, \quad (4)$$

where $r_0^{ij} = x^i - x^j$, $r_1^{ij} = y^i - y^j$, $\phi_r = \partial\phi/\partial r$, and $\phi_{rr} = \partial^2\phi/\partial r^2$. Our focus is on tracking the evolution of the smallest nonzero eigenvalue of the Hessian, λ_{\min} , and the corresponding eigenmode, during the AQE.

III. BACKGROUND: THE SQUARE ROOT SINGULARITY

Here, we briefly sketch the derivation of the square-root singularity. Because of the presence of disorder, the bulk modulus and other nonlinear moduli will have two contributions, one coming from the variation of the potential energy with changing deformation (well-known in the literature as the Born term) and the contribution coming from the non-affine motions of particles. Note that, at zero temperature, this nonaffine contribution in a perfect crystal will not be there. The nonaffine part of the contribution is one that is responsible for the observed square-root singularity in these moduli. For example, bulk modulus will have a nonaffine contribution which will diverge as $\sim 1/\lambda_{\min}$, whereas the next-order nonlinear modulus will diverge as $\sim 1/\lambda_{\min}^3$. Now as these two moduli will be related to each other via a simple derivative with respect to the applied strain, one can clearly see that $\lambda_{\min} \sim \sqrt{\gamma_p - \gamma}$, where γ_p is the strain at which the plastic drop happens. A detailed derivation can be found in Ref. [29]. In our current paper, γ will be inversely related to the density change, so one expects naturally to see $\lambda_{\min} \sim \sqrt{\rho - \rho_c}$, where ρ_c is the density at which the plastic event happens.

IV. RESULTS

A. The yielding

When we expand the homogeneous solid, the density decreases and expectedly the pressure also decreases; see Fig. 1(a) for the density dependence of the ensemble-averaged pressure $\langle P \rangle$ for different system sizes. Energy of the system $\langle U/N \rangle$ also decreases simultaneously; see Fig. 1(b). As expansion continues, beyond some density, the pressure becomes

negative, implying occurrence of internal tension. When the pressure changes signs, the energy goes through a minimum and then starts increasing. Eventually, the built-up tension is released, and the system yields with a big jump in pressure [see Fig. 2(a) for the case of a trajectory corresponding to $N = 10^5$]. The fluctuations in pressure within the ensemble, quantified via a susceptibility $\chi_p = N(\langle P^2 \rangle - \langle P \rangle^2)$, goes through a maximum when the jump in pressure is witnessed; see Fig. 1(c). The pressure jump and a peak in the corresponding susceptibility parallels the response to shear, where a large stress drop at yielding is associated with a peak in stress fluctuations [45]. Similar behavior is also observed in the energy fluctuations, quantified via the susceptibility $\chi_u = (1/N)[\langle U^2 \rangle - \langle U \rangle^2]$; see Fig. 1(d).

We note that the jump in pressure becomes sharper with increasing system size. Along with that, the peak height of the susceptibility increases as $\chi_p^{\text{peak}} \sim N$ [see inset of Fig. 1(c)], with the peak also becoming narrower, similar to what has been observed in the case of AQS response [45]. These observations evidence the existence of a yielding transition, located at the density at which χ_p^{peak} occurs, with the yield point shifting to larger densities with increasing N [see Fig. 1(e)].

We now focus on the spatial ramifications of the response to the AQE process by illustrating the evolution of an example particle configuration, whose P versus ρ trajectory is shown in Fig. 2(a). We observe that the state which is spatially homogeneous at higher density [see Fig. 2(b)] yields under expansion via the spontaneous formation of a large cavity, as shown in Fig. 2(b). Upon further expansion, the cavity increases in size and newer cavities appear in front of the expanding front [see Figs. 2(d) and 2(e)], with these events showing up as saw-toothed steps in the P versus ρ as shown in Fig. 2(a) [18]. While the expansion proceeds, cavities start merging, the fracture expands and eventually percolates, leading to the complete failure of the system [46,47]; see Figs. 2(f) and 2(g). The processes of cavity mergers and eventual fracture via fissures of necklike structures lead to large fluctuations in pressure which shows up as a secondary peak in χ_p , very distinctively visible for larger system sizes ($N = 10^5, 2.5 \times 10^4$). Here too, we notice that the location of the peak shifts to larger density with increasing system size [38]. We note that these processes also happen in the smaller system and the second peak in χ_p is likely to occur there too, probably at smaller ρ .

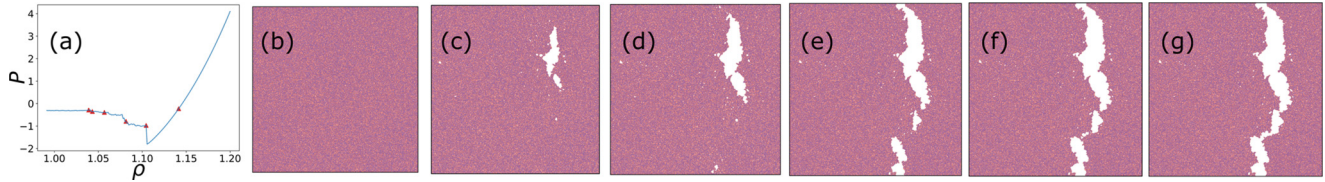


FIG. 2. Model KABLJ. (b)–(g) Snapshots from a $N = 10^5$ system showing cavitation and eventual failure at density points $\rho = 1.143$ (b), 1.106 (c), 1.083 (d), 1.058 (e), 1.043 (f), 1.039 (g) as marked for the single trajectory for which the evolution of pressure with density is shown in (a).

B. Postyield analysis

Next, we probe the stability of the local minima visited by the amorphous system during the quasistatic expansion, focusing on the density regime around yielding and beyond, prior to the complete fracture. For this purpose, we compute the smallest nonzero eigenvalue, λ_{\min} , of the Hessian matrix of the configuration obtained after each combined step of expansion and minimization. In Fig. 3(a), the evolution of λ_{\min} with ρ is plotted for a $N = 5000$ KABLJ state, using an expansion step of $\epsilon = 5 \times 10^{-4}$ for the expansion trajectory shown in Fig. 3(b) initiated from $\rho = 1.2$. We note that for every jump in pressure, λ_{\min} drops sharply. When well-resolved via smaller expansion steps ranging between 10^{-8} to 10^{-11} , λ_{\min} vanishes as a power law: $\lambda_{\min} \sim \sqrt{(\rho - \rho_c)/\rho_c}$, where ρ_c is the estimated location, in each case, of the plastic instability marked by the square-root singularity. In Fig. 3(c), the power-law behavior of λ_{\min} is displayed in the vicinity of the density locations marked in Fig. 3(b), which correspond to the estimated ρ_c obtained via the power-law fit in each case; see data set labeled (1). These locations correspond to the sequence of initial cavitation, subsequent increase in the cavity, and also formation of neighboring cavities; see SM [38] for the density maps. The vanishing of λ_{\min} , in each case, is thus consistent with the scenario of saddle-node bifurcation discussed in Sec. I. Thus, for each of these irreversible events, the nature of the singularity is exactly the same, and this is observed for all system sizes as shown in the SM [38]. In Fig. 3(c), we also show that the same power-law behavior is observed for other model glass-forming systems in similar density regimes, both in $d = 2$ and 3 , thus underlining the universal nature of this finding across amorphous systems. Note that the data are scaled appropriately with respective proportionality constants (A) to collapse the curves of the same model on top of each other.

Next, if we plot the eigenfunction corresponding to the minimum eigenvalue at the brink of singularity, i.e., the last numerically resolved density prior to ρ_c , we observe that its spatial structure is very similar to the nonaffine displacement field that is generated during the expansion step on the approach to ρ_c , i.e., between the last two numerically resolved density points prior to the singularity. In Figs. 3(d) and 3(e), we demonstrate this for the events marked in Fig. 3(a) during the postyield regime. This clearly demonstrates that just the lowest eigenmode of the Hessian matrix contributes to the ensuing plastic instability, i.e., there exists only one unstable direction on the energy landscape, viz. the one provided by the eigenvector corresponding to λ_{\min} .

To summarize, despite the occurrence of density inhomogeneities, for all such events in this regime around yielding

and prior to complete fracture, plastic events are generically approached by incidents of saddle-node bifurcation within the underlying potential energy landscape, similar to what has been earlier observed during the response to quasistatic shear [24,27,30]. Thus, one can conclude that such singularities are characteristic of plastic events whenever an amorphous solid responds to large mechanical deformations, be it via shear or expansion.

C. Analyzing the yielding avalanche

In the previous subsection, we discussed the displacement fields at the brink of the plastic instability, i.e., approaching each ρ_c from a slightly larger density. Now, we focus on the displacement field across the plastic instability, i.e., the pressure jump. In particular, we discuss the case of the main cavitation event marked in Fig. 3(a), occurring at $\rho_c \approx 1.09489$, for which we show in Fig. 4(c) the spatial map of displacement field associated with the emergence of the large cavity. We contrast this with the spatial map of eigenvector [Fig. 4(a)] related to λ_{\min} , at the brink of the event, i.e., the last numerically resolvable point prior to the corresponding ρ_c , viz. at a distance of $\delta\rho \approx 10^{-9}$ from the instability. The overlap between the maps in (a) and (c) is 0.57. On the other hand, for the displacement field on the brink of these events, viz. between the last two numerically resolved data points on the power-law branch prior to the event, the overlap is 0.99; see Fig. 4(b) for the displacement field. Thus, although the approach to the instability is solely determined by the eigenmode related to λ_{\min} , the displacement across the plastic drop has a more avalanche-like character wherein a cascade of plastic events, triggered via the first event, occur before stability is regained on the landscape. Such an avalanche-like feature has also been reported in the case of sheared amorphous solids during the occurrence of large stress drops [48], again underlying the similar behavior for two different mechanical deformation protocols.

D. Statistics of plastic events

We now study the statistics of the jumps in pressure and energy, in the density regime beyond yielding, for the different system sizes, to probe the system size scaling behavior of the distributions of pressure and energy jumps, ΔP and ΔU , respectively. We note that, in this regime, both pressure and energy are not in a true stationary state. Nevertheless, we try to get some idea about the scale of the avalanches as the system transits toward eventual failure after a spot of weakness has been seeded in the form of a cavity.

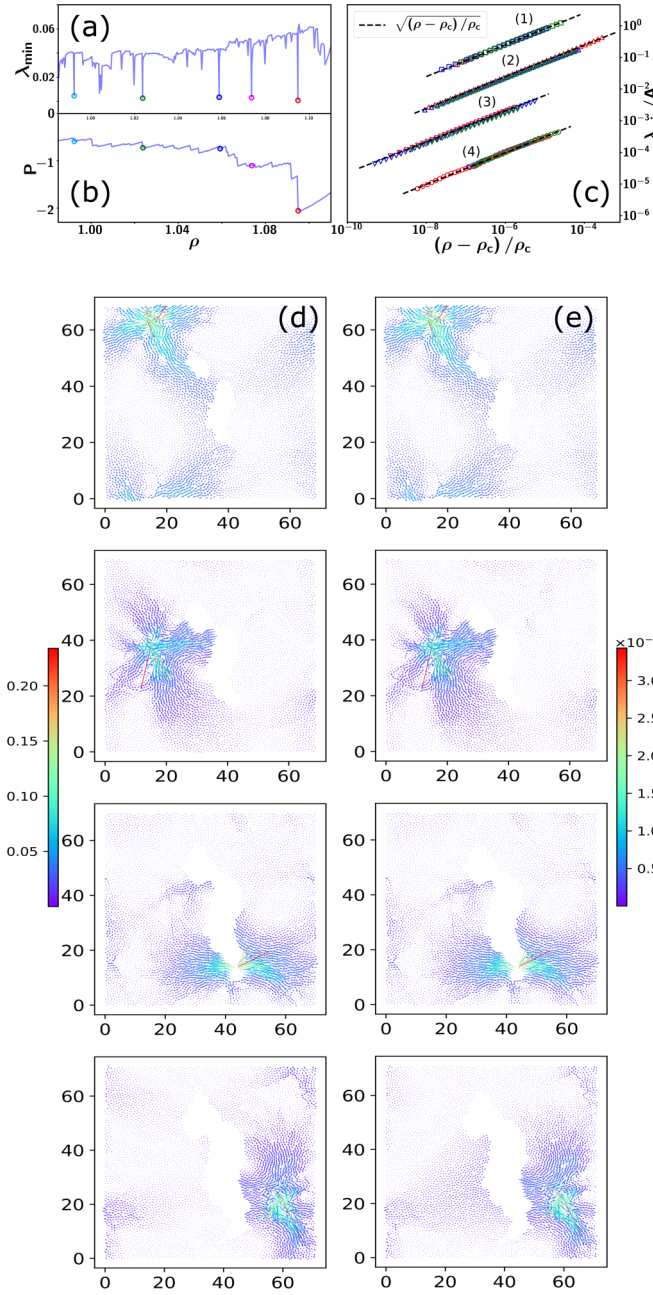


FIG. 3. Variation of the (a) minimum eigenvalue of the Hessians, λ_{\min} and (b) corresponding pressure during a particular quasistatic expansion trajectory of a $N = 5000$ KABLJ state. (c) For amorphous states obtained at density points marked in (a) and (b), λ_{\min} shows power-law behavior $\lambda_{\min} \propto \sqrt{(\rho - \rho_c)/\rho_c}$, where ρ_c is the estimated location of singularity in each case (dataset labeled as 1). Also shown are similar power laws obtained in other $d = 2, 3$ models [38]; data sets labeled as 2 (3dKABLJ), 3 (3dWahn), 4 (2dLancon). Note that the data are scaled appropriately with respective proportionality constants (A) to collapse the curves of the same model on top of each other. (d) For the density locations in the postyield regime, marked in (a), maps of nonaffine displacements on the approach to ρ_c . (e) Corresponding maps of eigenfunctions associated with respective λ_{\min} .

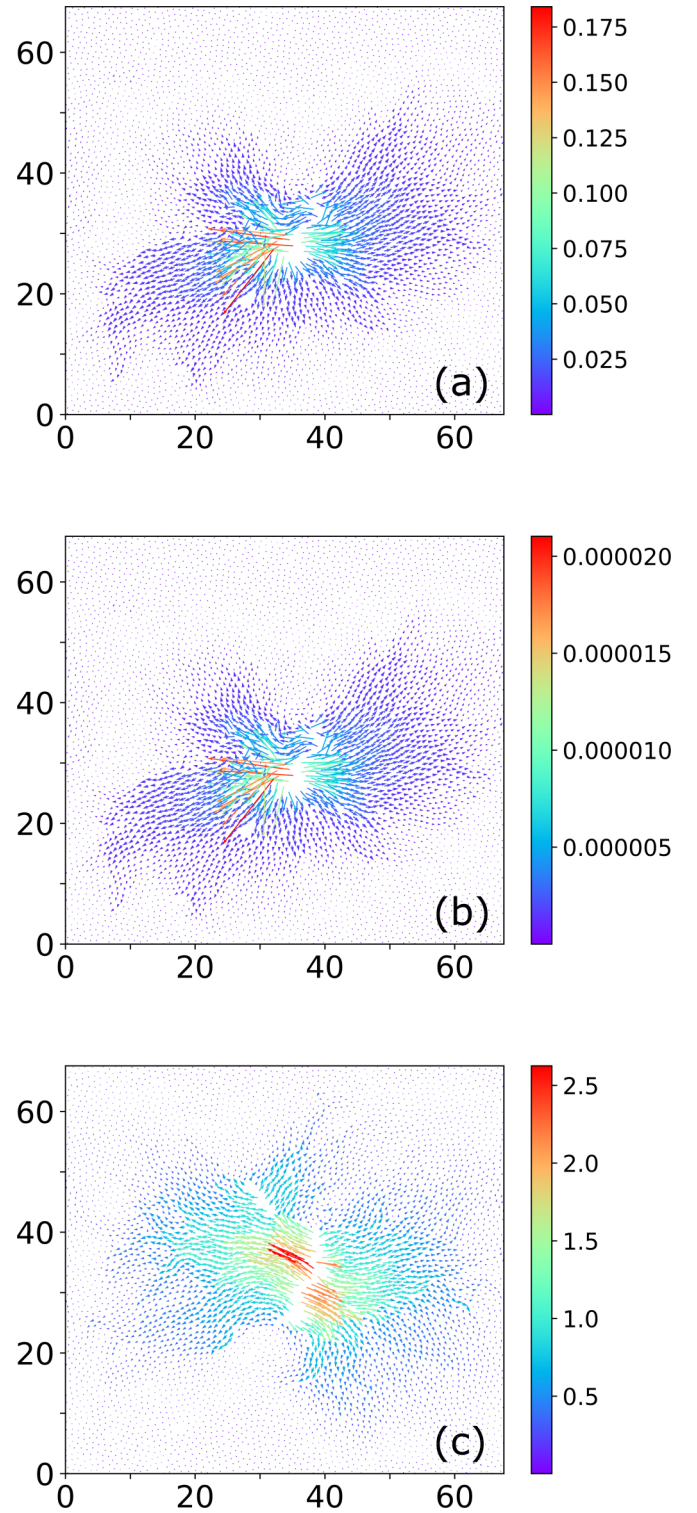


FIG. 4. The yielding avalanche. On the approach to the main cavitation event, for the trajectory shown in Fig. 3(a), at $\rho_c \approx 1.09489$ —(a) the eigenmode measured at the last numerically resolved density prior to the yielding event, viz. at a distance of $\delta\rho \approx 10^{-9}$; (b) the corresponding displacement field while approaching the yield point. (c) The displacement field across the subsequent yielding event leading to cavitation.

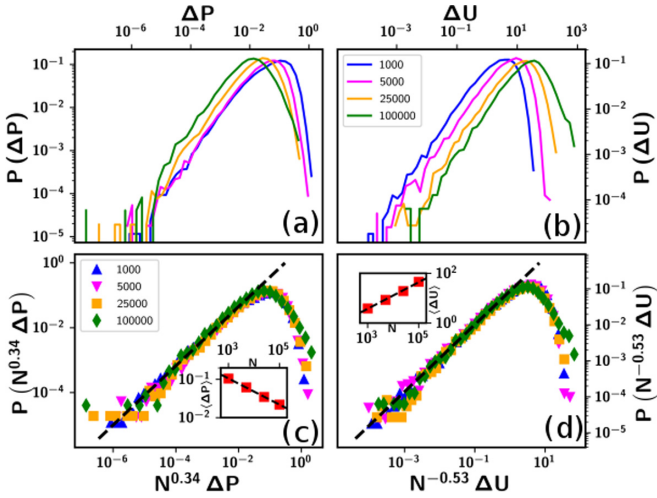


FIG. 5. Model KABLJ. Top: Distribution of jumps in (a) pressure and (b) energy, during AQE, after occurrence of main cavitation event. Bottom: Data collapse of the distributions, with appropriate N -scaling, which also reflects in the system size dependence of corresponding mean jump values, viz. $\langle \Delta P \rangle \sim N^{-0.34}$ (c), $\langle \Delta U \rangle \sim N^{0.53}$ (d), shown in the respective insets. The dashed lines in bottom panel correspond to power-laws with exponents 0.91 (c) and 0.93 (d).

The distributions, $P(\Delta P)$ and $P(\Delta U)$, for the different N are shown in Figs. 5(a) and 5(b). The distributions for different N collapse upon scaling the argument by $N^{-0.34}$ and $N^{0.53}$, respectively; see Figs. 5(c) and 5(d), which is also reflected in the N dependence of the first moments of the distributions, viz. $\langle \Delta P \rangle$ and $\langle \Delta U \rangle$, as shown in the respective insets. We note that for the smaller system sizes, these distributions are independent of the sampling window, postcavitation (see SM [38]). However, for the larger systems, there is a density window where these distributions deviate and this happens near the second peak in χ_p where larger events tend to happen due to fissures and mergers; post this regime, the distributions recover the scaling form. However, the vestiges of large drops in pressure and energy do show up in the tails of the distributions aggregated across the density regime after yielding; see Figs. 5(a), 5(b) and SM [38].

It is to be noted that the scaling exponents are different from the case of shear and also the difference between these exponents comes out to be ≈ 0.9 unlike in the case of yielding under shear, where $\alpha - \beta \approx 1$. However, the latter holds only when the density does not change [49], which is the case for shear but not for expansion. Moreover, the distributions themselves show nice power-law behavior at small arguments as $P(\Delta P) \sim \Delta P^\eta$ and $P(\Delta U) \sim \Delta U^\theta$, with $\eta \simeq 0.91$ and $\theta \simeq 0.93$ as shown in Figs. 5(c) and 5(d) by the solid lines. It also seems that the forms of the distributions can be approximated by the Weibull distribution with similar power-law exponents; see SM [38]. It is not immediately obvious why pressure and energy drops in the postyield should show extreme value statistics which is expected for the first plastic drop as shown before for AQS studies [30]. The power-law exponent of $P(\Delta U)$ suggests an exponent 0.52 for the system-size dependence of $\langle \Delta U \rangle$ in agreement with our observation but the pressure drop statistics does not follow the same. This observation does warrant further studies for better

understanding plastic instabilities during AQE. Nevertheless, the scaling collapse of distributions suggests that under AQE, postyield, amorphous solids display scale-free plasticity too, just like in the case of AQS albeit with different value of exponents α and β .

E. Analysis of the first event

So far, we have focused on the events after yielding, i.e., the main cavitation process. Now we probe the first instance when λ_{\min} vanishes, i.e., occurrence of the first irreversible plastic event, during the expansion process, starting from the high density state. We observe that this instability occurs at a fairly large density, far away from cavitation; see Fig. 6(a) for a single trajectory of a $N = 5000$ system. By sampling such events from several trajectories, we show in Fig. 6(b) that here too $\lambda_{\min} \sim \sqrt{(\rho - \rho_c)}/\rho_c$, underlying that all such instabilities have a similar origin, viz, a saddle-node bifurcation in the underlying energy landscape. The spatial map of the eigenfunction at the brink of the instability illustrated in Fig. 6(a) is shown in Fig. 6(c). Again it matches well with the nonaffine displacement undergone on the approach to the instability [see Fig. 6(d)], with both showing system-spanning spatial structures having a quadrupolar Eshelby-like shape [2,24]. We note that even in the case of response to shear, preyielding avalanches have been reported [50]. Unlike the case at cavitation, no spatial inhomogeneity in density occurs here; see Fig. 6(e). In fact, in between this first event and yielding via cavitation, numerous plastic events occur, and in each case, the nature of the singularity is the same. The corresponding spatial maps of nonaffine displacements initially show Eshelby-like shapes, which somewhat get distorted as the cavitation regime is approached (see SM [38]), and at cavitation and beyond take a different structure in the vicinity of the cavity, as is visible in Fig. 3(e). The shear mode visible during the early events is perhaps caused by the frozen-in shear stresses generated during the preparation of the glass via quench. It is possible that it takes several events to relax out these frozen-in stresses and thereafter as the cavitation regime is approached, the shape of the eigenmodes start to deviate with possible mixing with the dilatational modes which become predominant at cavitation (see SM [38]). Even beyond yielding, the emerging solid matrix has a higher density wherein Eshelby-like events can again occur upon further deformation. Systematic investigations of these eigenfunctions needs to be done in future.

V. CONCLUSIONS

To summarize, we have studied how a spatially homogeneous amorphous solid responds to quasistatic isotropic expansion. As expected, the release of built-up internal stresses leads to yielding transition via cavitation, which then acts as precursor to eventual failure via system-spanning fracture. Both the yielding density as well as the location of complete fracture can be identified via susceptibility measurements. The system-size scaling of χ_p is exactly the same as that observed for applied shear.

Our main focus is in examining the stability of the local minima that the system visits during the expansion process

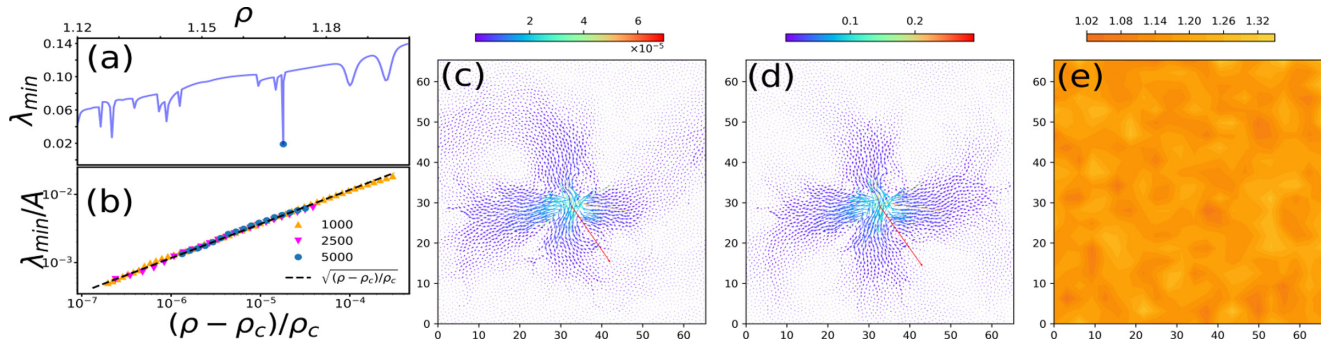


FIG. 6. Model KABLJ. (a) Variation of λ_{\min} for an expansion trajectory ($N = 5000$), with the location of first event marked. (b) For first plastic events sampled from independent trajectories, power-law behavior: $\lambda_{\min} \propto \sqrt{(\rho - \rho_c)/\rho_c}$. Data shown for different system sizes, as marked, and scaled appropriately for the data collapse. (c) Map of the eigenfunction related to λ_{\min} at the brink of $\rho \approx \rho_c (= 1.168)$ corresponding to trajectory shown in (a). (d) Map of corresponding nonaffine displacement field. (e) Coarse-grained density field after the first jump, displaying spatial homogeneity.

by monitoring the smallest eigenvalue of the corresponding Hessian matrix. We demonstrate, using several model amorphous solids, both in $d = 2$ and 3, that whenever the eigenvalue goes through zero, all throughout the expansion trajectory, be it for the first event in the high density phase or around and after the yielding via cavitation, it vanishes as a square-root singularity, which is characteristic of a saddle-node bifurcation within the underlying energy landscape. Thus, the point of yielding, where such instability was reported for a monocomponent system [32], is nothing special vis-à-vis how the eigenvalue vanishes. Rather, these irreversible processes, which lead to nonaffine displacements, seem universal characteristics of plastic events whenever an amorphous solid responds to large mechanical deformations, be it via shear or expansion. However, we note that unlike yielding via shear which can occur in amorphous materials

of all kinds, cavitation has a thermodynamic underpinning vis-à-vis the existence of gas-solid coexistence in the phase diagram of attractive glass-formers [51] and not for repulsive ones.

In the future, we plan to study the statistics of the first and subsequent intermediate events prior to cavitation to connect with similar analysis done for AQS response.

ACKNOWLEDGMENTS

We thank the HPC facility at IMSc-Chennai for providing computational resources. S.K. would like to acknowledge the support from Swarna Jayanti Fellowship Grants No. DST/SJF/PSA-01/2018-19 and No. SB/SFJ/2019-20/05. We thank Alberto Rosso, Damien Vandembroucq, Lisa Manning, and Peter Sollich for useful discussions.

- [1] R. Zallen, *The Physics of Amorphous Solids* (WILEY-VCH Verlag GmbH & Co. KGaA, Weinheim 2008).
- [2] J.-L. Barrat and A. Lemaitre, *Dyn. Heterog. Glasses, Colloids, Granular Media* **150**, 264 (2011).
- [3] D. Rodney, A. Tanguy, and D. Vandembroucq, *Modell. Simul. Mater. Sci. Eng.* **19**, 083001 (2011).
- [4] A. Nicolas, E. E. Ferrero, K. Martens, and J.-L. Barrat, *Rev. Mod. Phys.* **90**, 045006 (2018).
- [5] M. Jiang, G. Wilde, J. Chen, C. Qu, S. Fu, F. Jiang, and L. Dai, *Acta Mater.* **77**, 248 (2014).
- [6] E. Bouchaud, D. Boivin, J.-L. Pouchou, D. Bonamy, B. Poon, and G. Ravichandran, *Europhys. Lett.* **83**, 66006 (2008).
- [7] Y. Shao, G.-N. Yang, K.-F. Yao, and X. Liu, *Appl. Phys. Lett.* **105**, 181909 (2014).
- [8] G. Wang, D. Q. Zhao, H. Y. Bai, M. X. Pan, A. L. Xia, B. S. Han, X. K. Xi, Y. Wu, and W. H. Wang, *Phys. Rev. Lett.* **98**, 235501 (2007).
- [9] F. Célerié, S. Prades, D. Bonamy, L. Ferrero, E. Bouchaud, C. Guillot, and C. Marlière, *Phys. Rev. Lett.* **90**, 075504 (2003).
- [10] C. Guerra, J. Scheibert, D. Bonamy, and D. Dalmas, *Proc. Natl. Acad. Sci.* **109**, 390 (2012).
- [11] Z. Lu, K.-i. Nomura, A. Sharma, W. Wang, C. Zhang, A. Nakano, R. Kalia, P. Vashishta, E. Bouchaud, and C. Rountree, *Phys. Rev. Lett.* **95**, 135501 (2005).
- [12] P. Murali, T. F. Guo, Y. W. Zhang, R. Narasimhan, Y. Li, and H. J. Gao, *Phys. Rev. Lett.* **107**, 215501 (2011).
- [13] I. Singh, R. Narasimhan, and U. Ramamurty, *Phys. Rev. Lett.* **117**, 044302 (2016).
- [14] F. R. Young *Cavitation* (Imperial Coll. Press, London, 1989).
- [15] P. H. Mott, A. S. Argon, and U. W. Suter, *Philos. Mag.* **A 68**, 537 (1993).
- [16] J. Rottler and M. O. Robbins, *Phys. Rev. E* **68**, 011801 (2003).
- [17] L.-Q. Shen, J.-H. Yu, X.-C. Tang, B.-A. Sun, Y.-H. Liu, H.-Y. Bai, and W.-H. Wang, *Sci. Adv.* **7**, eabf7293 (2021).
- [18] Y. E. Altabet, F. H. Stillinger, and P. G. Debenedetti, *J. Chem. Phys.* **145**, 211905 (2016).
- [19] Y. E. Altabet, A. L. Fenley, F. H. Stillinger, and P. G. Debenedetti, *J. Chem. Phys.* **148**, 114501 (2018).
- [20] V. Testard, L. Berthier, and W. Kob, *Phys. Rev. Lett.* **106**, 125702 (2011).
- [21] P. Guan, S. Lu, M. J. B. Spector, P. K. Valavala, and M. L. Falk, *Phys. Rev. Lett.* **110**, 185502 (2013).
- [22] P. Chaudhuri and J. Horbach, *Phys. Rev. B* **94**, 094203 (2016).
- [23] K. Paul, R. Dasgupta, J. Horbach, and S. Karmakar, *Phys. Rev. Res.* **2**, 042012(R) (2020).
- [24] C. E. Maloney and A. Lemaitre, *Phys. Rev. E* **74**, 016118 (2006).

- [25] S. Karmakar, E. Lerner, I. Procaccia, and J. Zylberg, *Phys. Rev. E* **82**, 031301 (2010).
- [26] C. Liu, E. E. Ferrero, F. Puosi, J.-L. Barrat, and K. Martens, *Phys. Rev. Lett.* **116**, 065501 (2016).
- [27] D. L. Malandro and D. J. Lacks, *J. Chem. Phys.* **110**, 4593 (1999).
- [28] C. Maloney and A. Lemaître, *Phys. Rev. Lett.* **93**, 016001 (2004).
- [29] S. Karmakar, E. Lerner, and I. Procaccia, *Phys. Rev. E* **82**, 026105 (2010).
- [30] S. Karmakar, E. Lerner, and I. Procaccia, *Phys. Rev. E* **82**, 055103(R) (2010).
- [31] J. Chatteraj, O. Gendelman, M. Pica Ciamarra, and I. Procaccia, *Phys. Rev. Lett.* **123**, 098003 (2019).
- [32] M. Shimada and N. Oyama, Gas-liquid phase separation at zero temperature: Mechanical interpretation and implications for gelation, [arXiv:2011.1248](https://arxiv.org/abs/2011.1248).
- [33] S. Sastry, P. G. Debenedetti, and F. H. Stillinger, *Phys. Rev. E* **56**, 5533 (1997).
- [34] S. Sastry, *Phys. Rev. Lett.* **85**, 590 (2000).
- [35] W. Kob and H. C. Andersen, *Phys. Rev. E* **51**, 4626 (1995).
- [36] B. P. Bhowmik, P. Chaudhuri, and S. Karmakar, *Phys. Rev. Lett.* **123**, 185501 (2019).
- [37] R. Brüning, D. A. St-Onge, S. Patterson, and W. Kob, *J. Phys.: Condens. Matter* **21**, 035117 (2009).
- [38] See Supplemental Material at <http://link.aps.org/supplemental/10.1103/PhysRevE.106.055004> for details of parameter tuning and our particle-based simulations.
- [39] G. Wahnström, *Phys. Rev. A* **44**, 3752 (1991).
- [40] F. Lançon, L. Billard, and P. Chaudhari, *Europhys. Lett.* **2**, 625 (1986).
- [41] M. L. Falk and J. S. Langer, *Phys. Rev. E* **57**, 7192 (1998).
- [42] E. Polak and G. Ribiere, ESAIM: Mathematical modelling and numerical analysis, *Model. Math. Anal. Numer.* **3**, 35 (1969).
- [43] S. Plimpton, *J. Comput. Phys.* **117**, 1 (1995).
- [44] E. Anderson, Z. Bai, C. Bischof, S. Blackford, J. Demmel, J. Dongarra, J. Du Croz, A. Greenbaum, S. Hammarling, A. McKenney *et al.*, *LAPACK Users' Guide*, 3rd ed. (Society for Industrial and Applied Mathematics, Philadelphia, PA, 1999).
- [45] M. Ozawa, L. Berthier, G. Biroli, A. Rosso, and G. Tarjus, *Proc. Natl. Acad. Sci.* **115**, 6656 (2018).
- [46] E. Bouchbinder, T.-S. Lo, and I. Procaccia, *Phys. Rev. E* **77**, 025101(R) (2008).
- [47] E. Bouchbinder, T.-S. Lo, I. Procaccia, and E. Shtilerman, *Phys. Rev. E* **78**, 026124 (2008).
- [48] E. Stanifer and M. L. Manning, *Soft Matter* **18**, 2394 (2022).
- [49] E. Lerner and I. Procaccia, *Phys. Rev. E* **79**, 066109 (2009).
- [50] B. Shang, P. Guan, and J.-L. Barrat, *Proc. Natl. Acad. Sci.* **117**, 86 (2020).
- [51] Note, even for short-range attractive interactions which have possible liquid-solid coexistence in the athermal limit [19], we observe a fast tearing apart of the system, initiated by micro-cavitation [38].